

Quantum entanglement driven by electron-vibrational mode coupling

F. M. Souza,* P. A. Oliveira, and L. Sanz

Instituto de Física, Universidade Federal de Uberlândia, 38400-902 Uberlândia, MG, Brazil

(Dated: March 16, 2022)

In this work, we provided a proof-of-principle of efficient production of maximally entangled states using charged quantum dots coupled to vibrational modes. The physical system consists of two pairs of quantum dots, each pair with a single electron able to tunnel between the dots, thus encoding a qubit. The electrons, initially not coupled, interact with two bosonic vibrational modes. It is demonstrated that the electron-vibrational mode coupling drives to an effective electron-electron interaction, which is the main mechanism behind the formation of maximally quantum entangled electronic states. The effect of this coupling follows a non-monotonic behavior, which is explained through an effective hamiltonian which takes into account high order transition processes.

PACS numbers: 78.67.Hc, 03.65.Ud,

Keywords: quantum information with solid state qubits, entanglement manipulation, quantum dots.

I. INTRODUCTION

Semiconductor nanostructures have become a promising scenario for implementation of quantum computation, as originally proposed in the late 90s [1, 2]. These devices show high versatility in front of the wide set of degrees of freedom that can be used to encode a qubit [3]. Single qubit operations have been reported in several physical setups including the electronic spin $1/2$ states [4], where fast two-qubit gates have been implemented recently in silicon [5, 6]. Other possibilities for quantum computation in semiconductors include the single-triplet qubit states of two-electrons in GaAs [7, 8], the exchange-only qubit with spin states [9] and the charge degree of electrons [10, 11], among others.

Quantum dots (QDs) show interesting properties due to the confinement of particles. From all the possibilities, including optical quantum dots [12–14] and electronic spin [15], the interest on the physics of charged quantum dots has been increasing, once they are scalable systems where initialization and readout are possible through a process involving detection even of a single electron [16, 17]. In this physical system, the qubits are defined based on the property of electronic tunneling [18, 19], with the single-qubit operations being controlled by this effect, together with the manipulation of the electronic detuning [18, 19]. The single-molecule electronics has been an outstanding issue due to its future implementations feasibility of a cheaper and faster single-electron transistor [20, 21].

To further increase the functionalities of a qubit with electrons in a quantum dot, it is interesting to check coupling effects to nanomechanical degrees of freedom [22–24]. This kind of interaction plays a significant role, bringing a wealth of interesting effects, such as quantum-shuttles in QDs [25–27], local cooling [28], phonon-assisted transport in molecular quan-

tum dot junctions [29, 30], and Franck-Condon blockade [31], among others. One possibility is the use of carbon nanotubes (CNT), one of the most successful new materials in view of their broad set of direct applications [32]. When operated as mechanical resonators, nanotubes show high quality factors [24, 33, 34] being possible, for instance, to excite, detect and control specific vibrational modes of a CNT with a current being injected from a scanning tunneling microscopy (STM) tip into a CNT [35]. Also, CNT can be used in the implementation of ultrahigh tunable frequency resonators [36–38], nanoradios [39], ultrasensitive mass sensors [40, 41], and it has been reported strong coupling regimes between single-electron tunneling and nanomechanical motion on a suspended nanotube, tuned via electrical gates [42]. Regarding applications in micro and nanoelectronics, carbon nanotubes present ballistic conduction [43] and Coulomb blockade effect in single and double nanotube based quantum dot devices [44]. Particularly, it was proposed a mechanically induced two-qubit quantum gate and the generation of entanglement between electronic spin states in CNT [45] and showed its potential as “flying” qubits for electron spin communications over long distances [36].

From the theoretical point of view, one successful model to explore the problem of a two-level system interacting to bosons was proposed by Rabi [46, 47], which can be treated both numerical and analytically [48–51]. A specific approximation, the Jaynes-Cummings (JC) model, becomes the theoretical support behind several quantum phenomena, including the formation of Schrödinger cats and quantum logic gates [52, 53]. The Rabi and JC model have been used in the context of the qubits coupled with bosons [54, 55], where this type of coupling become responsible by single-qubit operations. Alternatively, the interaction between particles and bosonic fields can result in the formation of polarons [56, 57]. Codifying a qubit as a polaron becomes a challenge, once the electron-phonon interaction is generally a mechanism of decoherence [58–60], although it was shown that this type of interaction can be used to build

* fmsouza@ufu.br

a quantum dot maser [54]. In what concerns the problem of quantum correlations emergence between qubits, mediated by bosonic modes, some theoretical works are found in literature [61–63]. In recent experimental works, the generation of quantum correlations is demonstrated considering the coupling of exciton with phonons [64]. Other possibility is the use of the coupling with photons [65] to control a two-qubit operation.

In this work, we investigate a system composed of two charge qubits interacting with each other via electron-vibrational mode coupling. The main goal of our study is to provide a proof-of-principle that electrons in quantum dots, coupled to high-frequency bosonic nanoresonators, can be used to generate maximally entangled states of charge qubits. The role of the electron-boson interaction is quite different in charge qubits if compared to the spin two-qubits scenario, once in charged quantum dots, this interaction preserves the state of a single qubit on the electronic degree of freedom, while creates or annihilates an excitation in the bosonic space.

The paper is organized as follows. In Sec. II, by using the unitary transformation of Lang-Firsov, we demonstrate that the electron-vibrational mode coupling is responsible for the occurrence of an effective electron-electron interaction. Then, we demonstrate how to encode two electronic qubits in our physical system. Section III is devoted to the exploration of the signatures of this effective interaction and correlated phenomena on the spectrum and eigenstates of the model. In Sec. IV, using as reference our previous work on quantum dynamics on coupled quantum dots [66, 67], we study the formation of maximally entangled electronic states under specific conditions. The feasibility and robustness against charge dephasing, the main decoherence process in the physical system of our proposal, is discussed in Sec. V. Section VI contains our final remarks.

II. MODEL

Our model consist of a multipartite system with two main parts, as illustrated in Fig. 1: the electronic subspace \mathcal{D} with two pairs of quantum dots, each pair with potential to encode a qubit, and the subspace \mathcal{V} , with two devices containing vibrational modes. Here, the vibrational mode 1 (VM1) couples to the electronic degrees of freedom of dots 1 and 3, while the vibrational mode 2 (VM2) couples to dots 2 and 4. Tunnelling is allowed between dots 1 (3) and 2 (4), being responsible for flipping the electronic state, if a qubit is encoded on a pair of dots. That means that the electron-bosonic field interaction does not fulfill this role, in contrast to the Rabi model.

Concerning the computational basis, if we assume a single electronic level in a quantum dot, the elements of the basis have the general form $|n_1 n_2 n_3 n_4\rangle$, where each number indicates the occupation of the specific dot (0-empty and 1-occupied). Additionally, the vibrational

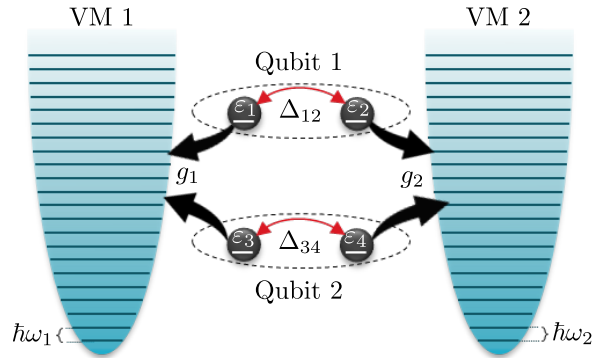


FIG. 1. Illustration of our system of interest: quantum dots 1 and 3 (2 and 4) are coupled with the vibrational (bosonic) mode VM1 (VM2) with frequency $\omega_{1(2)}$. Additionally, the dots 1 (3) and 2 (4) are coupled by tunneling with real parameter $\Delta_{12(34)}$, where ε_i is the electronic level of the n -th dot ($n = 1, \dots, 4$). If two quantum dots share a single electron, the system can encode a qubit, as shown by dashed lines.

subspaces are spanned by the occupation number basis states of the form $|ml\rangle_{\mathcal{V}}$, with $m, l = 0, 1, \dots, \infty$. Putting all together we end up with $|n_1 n_2 n_3 n_4\rangle_{\mathcal{D}} \otimes |ml\rangle_{\mathcal{V}} = |n_1 n_2 n_3 n_4, ml\rangle$ as a general element of the computational basis used to span the complete space.

A. General Hamiltonian

The Hamiltonian which describes the physical setup is written as

$$H = H_{\mathcal{D}} + H_{\mathcal{V}} + V_{\mathcal{D}\mathcal{V}}, \quad (1)$$

where $H_{\mathcal{D}}$ and $H_{\mathcal{V}}$ are the free Hamiltonians of the quantum dots and vibrational modes subspaces, respectively and $V_{\mathcal{D}\mathcal{V}}$ is the dots-vibrational modes coupling. The first term is written as:

$$H_{\mathcal{D}} = \left[\sum_{i=1}^2 \varepsilon_i N_i^{\mathcal{D}} + \Delta_{12} (S_1^{\dagger} S_2 + S_2^{\dagger} S_1) \right] + \left[\sum_{i=3}^4 \varepsilon_i N_i^{\mathcal{D}} + \Delta_{34} (S_3^{\dagger} S_4 + S_4^{\dagger} S_3) \right], \quad (2)$$

where S_i^{\dagger} (S_i) are the creation (annihilation) operators for the i -th quantum dot and $N_i^{\mathcal{D}} = S_i^{\dagger} S_i$. The parameters ε_i are the electronic levels for each dot while $\Delta_{12(34)}$ is a real number describing the tunnel coupling. If we consider a single vibrational mode per subsystem, the free Hamiltonian $H_{\mathcal{V}}$ becomes ($\hbar = 1$)

$$H_{\mathcal{V}} = \omega_{v_1} B_{v_1}^{\dagger} B_{v_1} + \omega_{v_2} B_{v_2}^{\dagger} B_{v_2}, \quad (3)$$

where ω_{v_j} is the energy of the corresponding j -th vibrational mode. Here $B_{v_j}^{\dagger}$ (B_{v_j}) creates (annihilates) an excitation in a j -th vibrational mode subspace. Finally, the

term $V_{\mathcal{D}\mathcal{V}}$, which provides the electron-vibrational mode coupling, is written as

$$V_{\mathcal{D}\mathcal{V}} = g_1 (N_1^{\mathcal{D}} + N_3^{\mathcal{D}}) \otimes (B_{v_1}^\dagger + B_{v_1}) + g_2 (N_2^{\mathcal{D}} + N_4^{\mathcal{D}}) \otimes (B_{v_2}^\dagger + B_{v_2}), \quad (4)$$

where parameter g_v gives the coupling strength between electronic and vibrational degrees of freedom.

B. Physical Parameters

In our calculations, we will assume realistic parameters, considering specifically the CNT scenario. We set all physical quantities in terms of the energies ω_v of the vibrational modes, once the comparisons of the tunneling and the electron-vibrational mode couplings in terms of ω_v become the key ingredients behind the generation of the electronic entangled states. We assume that both vibrational modes has the same frequency, i.e., $\omega_1 = \omega_2 = \omega$ [29], and set the frequency at $\omega = 20$ meV (4.8 THz), being in agreement with the high-frequencies values of the radial breathing mode [35]. The tunneling parameter is fixed at $\Delta_{12} = \Delta_{34} = 5 \times 10^{-3}\omega = 0.1$ meV, as reported in experiments on parallel CNT quantum dots [68]. In face of the potential of manipulation of the electron-phonon coupling in the context of quantum dots and nanotubes [42], we are interested in tuning g_v as done in some theoretical treatments [29, 30], from 0.1ω up to 0.5ω . The temperature is assumed to be low enough to guarantee that the dominant vibrational state is at $|0\rangle \otimes |0\rangle$. Typically, temperatures around $T = 5$ K are used in experiments on transport in CNT [35]. Finally, the values for the electronic levels, $\varepsilon_{i(j)}$ can be tuned via gate voltages applied on the quantum dots arrangement [19].

C. Effective Hamiltonians

It is interesting to obtain further insight on the system by exploring some analytical features of the full model. For instance, consider that the electron-vibrational mode coupling is the same for both vibrational modes so that, $g_1 = g_2 = g$ [69]. In order to analyze the action of electron-vibrational mode and tunnel couplings, we apply the Lang-Firsov [70] unitary transformation over the Hamiltonian in Eq.(1). This transformation is regularly used in the study of electron-phonon interaction, in the contexts of small-polaron models [71] and strong correlated systems [72].

We define the operator S as

$$S = \alpha (N_1^{\mathcal{D}} + N_3^{\mathcal{D}}) \otimes (B_{v_1}^\dagger - B_{v_1}) + \alpha (N_2^{\mathcal{D}} + N_4^{\mathcal{D}}) \otimes (B_{v_2}^\dagger - B_{v_2}), \quad (5)$$

with $\alpha = \frac{g}{\omega}$. The Lang-Firsov transformation consists on the calculation of the Hamiltonian $\bar{H} = e^S H e^{-S}$. Con-

sidering H as written in Eqs.(1-4), we find

$$\bar{H} = (\bar{H}_{\mathcal{D}} + V_{\text{eff}}) + H_{\mathcal{V}} + \Delta_{\mathcal{D}\mathcal{V}}^T, \quad (6)$$

where

$$\bar{H}_{\mathcal{D}} = \sum_{i=1}^4 \tilde{\varepsilon}_i N_i^{\mathcal{D}}, \quad (7)$$

is the transformed Hamiltonian for the dots with $\tilde{\varepsilon}_i$ being the shifted energy due to the action of the electron-vibrational mode coupling being $\tilde{\varepsilon}_i = \varepsilon_i - \alpha^2 \omega$. The term V_{eff} is an effective electron-electron interaction written as

$$V_{\text{eff}} = -2\alpha^2 \omega N_1^{\mathcal{D}} \otimes N_3^{\mathcal{D}} - 2\alpha^2 \omega N_2^{\mathcal{D}} \otimes N_4^{\mathcal{D}}, \quad (8)$$

and the last term

$$\Delta_{\mathcal{D}\mathcal{V}}^T = \left[\left(\Delta_{12} S_1^\dagger S_2 \right) + \left(\Delta_{34} S_3^\dagger S_4 \right) \right] \otimes \mathbb{D}_{12} + \left[\left(\Delta_{12} S_2^\dagger S_1 \right) + \left(\Delta_{34} S_4^\dagger S_3 \right) \right] \otimes \mathbb{D}_{12}^\dagger, \quad (9)$$

describes an effective electron-vibrational mode coupling. Here we have define the operator

$$\begin{aligned} \mathbb{D}_{12} &= e^{\alpha(B_{v_1}^\dagger - B_{v_1})} \otimes e^{-\alpha(B_{v_2}^\dagger - B_{v_2})} \\ &= D(\alpha) \otimes D(-\alpha), \end{aligned} \quad (10)$$

which is a tensorial product of displacement operators, as defined for the quantum harmonic oscillator [73]. The new transformed Hamiltonian, Eq. (6) and its terms Eqs. (7)-(9), highlights important effects of the couplings considered on this particular physical system. The first is a shift on the value of the electronic levels which depends on both, the coupling parameter g and ω . The second is the effective electron-electron interaction which couples the electrons from different qubits, which is mediated by the electron-vibrational mode coupling.

Now, we are ready to encode two qubits in our physical system, as sketched in Fig. 1. We assume that each pair of quantum dots (dots 1-2 and dots 3-4) contains a single electron. Therefore, we have a reduced electronic basis with four states of the form $|n_1 n_2 n_3 n_4\rangle$, namely, $|1010\rangle = |\uparrow\uparrow\rangle$, $|1001\rangle = |\uparrow\downarrow\rangle$, $|0110\rangle = |\downarrow\uparrow\rangle$ and $|0101\rangle = |\downarrow\downarrow\rangle$, where spin-1/2 notation was introduced. In this restricted space, we use the matrix representations of operators $N_i^{\mathcal{D}}$ and S_i to write the Hamiltonian, Eq.(9), as

$$\bar{H} = \bar{H}_0 + \bar{V}, \quad (11)$$

where

$$\bar{H}_0 = \left[\sum_{q=1}^2 \frac{\delta_q}{2} \sigma_z^{(q)} - \alpha^2 \omega (\sigma_z \otimes \sigma_z + I) \right] + H_{\mathcal{V}}, \quad (12)$$

and

$$\bar{V} = \sum_{q=1}^2 \Delta_q \left[\sigma_+^{(q)} \otimes \mathbb{D}_{12} + \sigma_-^{(q)} \otimes \mathbb{D}_{12}^\dagger \right], \quad (13)$$

where q runs over the electronic qubits, so for qubit $q = 1(2)$ the detuning is defined as $\delta_{1(2)} = \varepsilon_{1(3)} - \varepsilon_{2(4)}$ and the tunneling parameter is given by $\Delta_{1(2)} = \Delta_{12(34)}$. This particular form of our model is interesting, as it is able to reveal the emergence of an effective electronic interaction term, $\sigma_z \otimes \sigma_z$, in a similar way to the models describing the experiments in charged QD [19].

III. SPECTRAL ANALYSIS

We proceed to explore the characteristics of energy spectrum and eigenstates of the Hamiltonian, Eq.(1). We focus on how the interplay between g , the tunnel coupling and the detuning δ_i can yield to the generation of maximally entangled states. Along with the study of energy spectrum, we are interested on the entanglement properties of the eigenstates. It is well known that Coulomb interaction is behind the formation of entangled states in coupled quantum dots molecule [66, 74]. Because of the information provided by transformed Hamiltonian, Eq. (7), we expect the occurrence of signatures of the effective electron-electron interaction on the entanglement degree of the eigenstates.

To quantify the entanglement degree, the measurement of concurrence is evaluated, as defined by Wootters [75], which requires the calculation of the density matrix for each eigenstate. We define $\hat{\rho}_l = |\psi_l\rangle \langle \psi_l|$, where $|\psi_l\rangle$ is the l -th eigenstate of Hamiltonian (1). Then, we calculate the reduced 4×4 density matrix for the two qubits, by tracing out the degrees of freedom of the vibrational modes so $\hat{\rho}_{\mathcal{D},l} = \text{Tr}_{\mathcal{V}}[\hat{\rho}_l]$. An auxiliary Hermitian operator [76] is defined as $R_l = \sqrt{\sqrt{\hat{\rho}_{\mathcal{D},l}} \widetilde{\hat{\rho}_{\mathcal{D},l}} \sqrt{\hat{\rho}_{\mathcal{D},l}}}$, where $\widetilde{\hat{\rho}_{\mathcal{D},l}} = (\sigma_y \otimes \sigma_y) \hat{\rho}_{\mathcal{D},l}^* (\sigma_y \otimes \sigma_y)$, is the spin-flipped matrix with $\hat{\rho}_{\mathcal{D},l}^*$ being the complex conjugate of $\hat{\rho}_{\mathcal{D},l}$. Finally, the concurrence is calculated considering $C = \max(0, \lambda_1 - \lambda_2 - \lambda_3 - \lambda_4)$ where λ_k ($k = 1, \dots, 4$) is the k -th eigenvalue of the operator R_l in decreasing order.

Motivated by our previous work [66], which demonstrated that, by changing δ_q , it is possible to reach maximally entangled states in Coulomb interacting qubits, here we check the behavior of energy and concurrence as a function of δ_1 , for different values of δ_2 . To begin our analysis, it is instructive to write the free energies of the two qubit model, Eq. (12), neglecting the tunnel coupling ($\Delta_q = 0$), which results in the following expressions:

$$\begin{aligned} \varepsilon_{\uparrow\uparrow,ml} &= \frac{\delta_1 + \delta_2}{2} - 2\alpha^2\omega + (m+l)\omega \\ \varepsilon_{\downarrow\downarrow,ml} &= -\left(\frac{\delta_1 + \delta_2}{2}\right) - 2\alpha^2\omega + (m+l)\omega \\ \varepsilon_{\uparrow\downarrow,ml} &= \frac{\delta_1 - \delta_2}{2} + (m+l)\omega \\ \varepsilon_{\downarrow\uparrow,ml} &= -\left(\frac{\delta_1 - \delta_2}{2}\right) + (m+l)\omega. \end{aligned} \quad (14)$$

The above equations allow the discussion of some important features concerning the spectrum, which shed light

on the conditions for the formation of maximally entangled states. Notice that $\varepsilon_{\uparrow\uparrow,ml} = \varepsilon_{\downarrow\uparrow,ml}$ at $\delta_1 = 2\alpha^2\omega$ and $\varepsilon_{\downarrow\downarrow,ml} = \varepsilon_{\uparrow\downarrow,ml}$ at $\delta_1 = -2\alpha^2\omega$. At these δ_1 values we expect the appearance of anticrossings due to the tunneling term of the Hamiltonian, that couples states like $|\uparrow\uparrow, 00\rangle$ to $|\downarrow\uparrow, 00\rangle$ and $|\downarrow\downarrow, 00\rangle$ to $|\uparrow\downarrow, 00\rangle$. However, in terms of entanglement, it is expected a low value of concurrence, once the eigenstates would be separable. Additionally, we find $\varepsilon_{\uparrow\downarrow,ml} = \varepsilon_{\downarrow\uparrow,ml}$ at $\delta_1 = \delta_2$ and $\varepsilon_{\uparrow\uparrow,ml} = \varepsilon_{\downarrow\downarrow,ml}$ at $\delta_1 = -\delta_2$. The Hamiltonian does not provide a first order coupling between states such as $|\uparrow\downarrow, 00\rangle$ and $|\downarrow\uparrow, 00\rangle$. However, these states can be coupled via second order transitions. This means that if the system is initialized at $|\uparrow\downarrow, 00\rangle$, it can evolve to $|\downarrow\uparrow, 00\rangle$, passing through intermediate states such as $|\uparrow\uparrow, ml\rangle$ and $|\downarrow\downarrow, ml\rangle$. At this specific condition, highly entangled states can be formed due to virtual processes. This effect will be used to dynamically generate entangled states, as discussed in the next section.

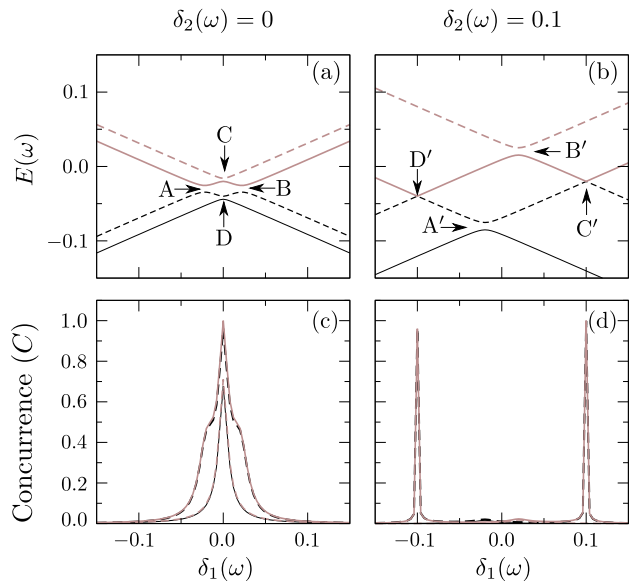


FIG. 2. Spectrum and entanglement degree as functions of δ_1 , of the first (solid black line), the second (dashed black line), the third (solid brown line) and the four (dashed brown line) eigenstate of the general Hamiltonian, Eq.(1). Here, it is shown (a) the energies and (b) the concurrence, considering $\delta_2 = 0$ and (c) energies and (d) concurrence, for $\delta_2 = 0.1\omega$. Anticrossings are indicated by arrows and identified with letters (see main text for details). Physical parameters are $g = 0.1\omega$ and $\Delta_1 = \Delta_2 = 5 \times 10^{-3}\omega$.

Fig. 2 shows the first four eigenvalues of the general Hamiltonian, Eq.(1), and the corresponding concurrences as functions of δ_1 , considering two different values of δ_2 . To perform our numerical calculation, both bases associated with the vibrational modes are truncated at $m_{\max} = l_{\max} = 13$. This number of computational states is enough to guarantee the accuracy of the lower eigenenergies. With respect to the energies, the results reported on Fig. 2(a)-(b) show anticrossings labeled with letters

(A,B) and (A',B'), corresponding to first order transitions that play a role at $\delta_1 = \pm 2\alpha^2\omega$. In contrast, the smaller anticrossings indicated by letters (C,D) and (C',D') are associated with second and higher order transitions that take place at $\delta_1 = \pm\delta_2$.

To understand what happens with the eigenvectors corresponding to the first order (A,B)-(A',B') and the second order anticrossings (C,D)-(C',D'), we use an stacked bar graph, Fig. 3(a)-(b). Each color and patterns corresponds to the population of a respective state of the 4D basis given by $\{|\uparrow\uparrow, 00\rangle, |\uparrow\downarrow, 00\rangle, |\downarrow\uparrow, 00\rangle, |\downarrow\downarrow, 00\rangle\}$, as indicated in the figure. The gray bar gives the sum of the populations of the remain components with at least one vibrational mode excitation. Comparing both types of anticrossings, we verified that the eigenstates in Fig. 3(a) are mainly superpositions of states, with at least one spin component at the same orientation, such as $|\uparrow\downarrow, 00\rangle$ and $|\downarrow\downarrow, 00\rangle$, or $|\downarrow\uparrow, 00\rangle$ and $|\uparrow\uparrow, 00\rangle$, which results in low entanglement. For clarity, in Appendix B we show the expansions of the eigenstates in the computational basis. In contrast, in Fig. 3(b) we find eigenstates such as $|\psi_{C-}\rangle$, $|\psi_{D+}\rangle$, $|\psi_{C'\pm}\rangle$ and $|\psi_{D'\pm}\rangle$ that are highly entangled eigenstates. For instance, $|\psi_{C'+}\rangle$ can be written with good accuracy as

$$|\psi_{C'+}\rangle = \frac{1}{\sqrt{2}} (|\uparrow\downarrow\rangle + e^{i\varphi} |\downarrow\uparrow\rangle) \otimes |00\rangle, \quad (15)$$

where φ is a relative phase. This shows that the electron-vibrational mode coupling is the source of the emergence of electronic Bell states as eigenstates.

In Fig. 2(c)-(d), we show the behavior of concurrence as a function of δ_1 . Note that C reaches values close to one, corresponding to the anticrossings (C, D) and (C', D'). This is consistent with the eigenstates $|\psi_{C-}\rangle$, $|\psi_{D+}\rangle$ for $\delta_2 = 0$, and $|\psi_{C'\pm}\rangle$ and $|\psi_{D'\pm}\rangle$ for $\delta_2 = 0.1\omega$, shown in Fig. 3. The eigenstate $|\psi_{C'+}\rangle$, in particular, presents the larger value of concurrence, $C \approx 1$. This fact is in agreement with an analytical solution (Appendix A) of the matricial representation of the general Hamiltonian, Eq.(1), in a rotated electronic basis of Bell states. Also, it is worthy to note that the condition $\delta_2 = 0.1\omega$, which results on the anticrossing C', favors an energetically isolated two-level subspace within $\{|\uparrow\downarrow, 00\rangle, |\downarrow\uparrow, 00\rangle\}$, which will be used in the next section in order to find an effective two-level model. Note also that we find $C \approx 0.9$ at anticrossings D and D'. By checking the values of the eigenstates coefficients, shown in Appendix B, we verified that although the electronic part is roughly similar to the Bell states $|\Phi_{\pm}\rangle$, as defined in Eq.(A1), the superposition has contributions from other electronic states, thus suppressing the degree of entanglement.

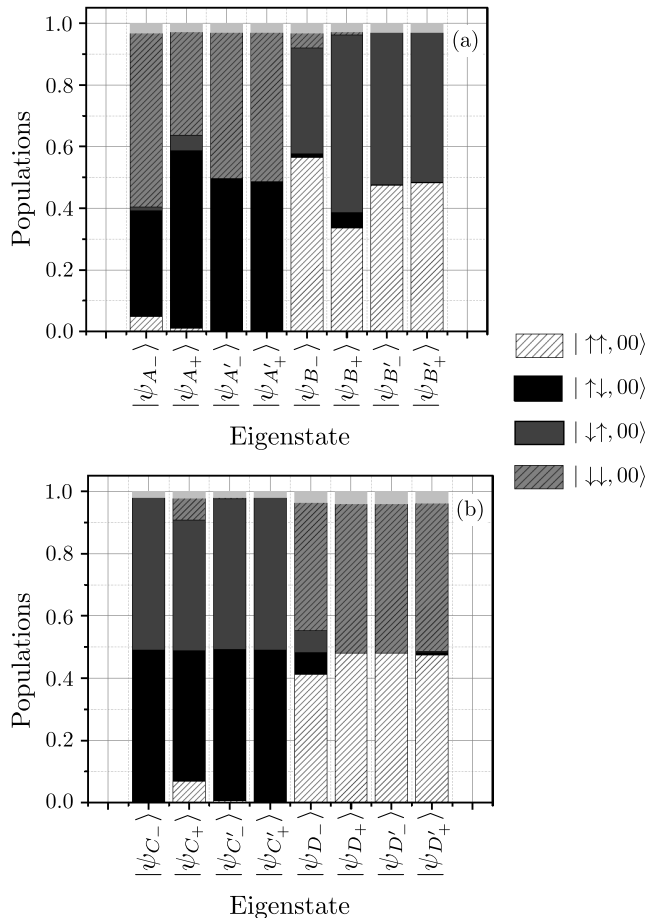


FIG. 3. Stacked bar graph showing the populations of states of the computational basis for the eigenstates at the anticrossing positions at Fig. 2 of: (a) first order and (b) second order. Color and patterns for the main contributors (states with $m = l = 0$) are described on the right side of the panel. Solid gray is used for the sum of the populations of other states. Physical parameters are $g = 0.1\omega$ and $\Delta_1 = \Delta_2 = 5 \times 10^{-3}\omega$.

IV. DYNAMICAL GENERATION OF MAXIMALLY ENTANGLED ELECTRONIC STATES

After studying the properties of the eigenstates of the model, we are ready to explore the generation of electronic entangled states by quantum dynamics with the general form,

$$|\Psi(\varphi)\rangle = \frac{1}{\sqrt{2}} (|\uparrow\downarrow\rangle + e^{i\varphi} |\downarrow\uparrow\rangle), \quad (16a)$$

$$|\Phi(\vartheta)\rangle = \frac{1}{\sqrt{2}} (|\uparrow\uparrow\rangle + e^{i\vartheta} |\downarrow\downarrow\rangle), \quad (16b)$$

where φ and ϑ are relative phases [77].

First, we obtain numerically the density operator $\rho(t) = |\psi(t)\rangle\langle\psi(t)|$, using the Hamiltonian (1), considering a specific initial state. Then, by tracing out the

vibrational degrees of freedom, we obtain the electronic reduced density matrix

$$\rho_{\mathcal{D}}(t) = \text{Tr}_{\mathcal{V}}[\rho(t)]. \quad (17)$$

The equation above is used to explore the dynamical behavior of the electronic part of the system, through the analysis of the evolution of the concurrence and the fidelity of the evolved state. The system is initialized at $\rho_0 = |\uparrow\downarrow, 00\rangle\langle\uparrow\downarrow, 00|$, where the vibrational part is experimentally feasible at low temperature (Sec. II B). This choice of ρ_0 is motivated by our findings concerning the anticrossing C' , which favors the generation of maximally entangled electronic states $|\Psi(\varphi)\rangle$. Analogously, the choice of $|\uparrow\uparrow, 00\rangle$ or $|\downarrow\downarrow, 00\rangle$ as initial states could result on the formation of entangled states of the form $|\Phi(\vartheta)\rangle$, for a dynamics considering the specific conditions of anticrossing D' . Any choice of initialization for the electronic state is realistic, once the experimental setup can be coupled to a set of auxiliary sources and drains of electrons, allowing charge injection at any of the quantum dots on the physical system.

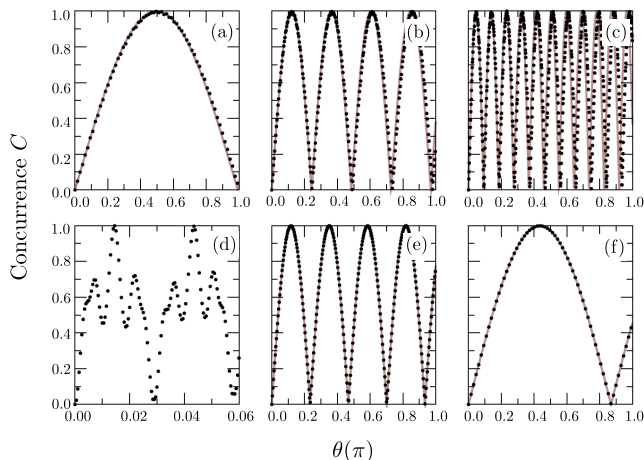


FIG. 4. Dynamics of the entanglement degree of the electrons as function of θ for different values of g , considering the physical parameters of the anticrossing C' : $\Delta = \Delta_1 = \Delta_2 = 5 \times 10^{-3}\omega$ and $\delta = \delta_1 = \delta_2 = 0.1\omega$. Here, the numerical calculation of C (black dots) and the analytic expression $C_{2ls}(t)$ as defined in Eq. (23) (brown line) are plotted considering (a) $g = 0.05\omega$, (b) $g = 0.10\omega$, (c) $g = 0.15\omega$, (d) $g = 0.22\omega$, (e) $g = 0.40\omega$, and (f) $g = 0.50\omega$.

Black dots in Fig. 4 show our numerical results for the entanglement dynamics considering the specific choice of parameters associated with the anticrossing C' , being $\Delta = \Delta_1 = \Delta_2$ and $\delta_1 = \delta_2 = 0.1\omega$, and different values of the electron-vibrational mode coupling g . We define a new time-dependent variable, $\theta = \Omega_0 t$, with $\Omega_0 = 2|\Delta|^2/\omega$, which will prove to be very useful in the discussion of the quantum dynamics of our system, as it will be noticed in the following discussions. Comparing the six panels, we notice that the concurrence C shows an oscillatory behavior, with its maximum value reaching

$C = 1$, indicating the formation of maximally entangled electronic states. Additionally, the period of the oscillations has a non-monotonic behavior as g increases. We identify three different situations: (i) for a first range of values of g ($g < 0.2\omega$) the system performs sinusoidal oscillations with a decreasing period as g increases, as can be seen in Figs. 4(a)-(c); (ii) there is an intermediate range of values of g where the dynamics do not correspond to a sinusoidal function, although they oscillate in a time scale significantly shorter (by two orders of magnitude) than the other cases, as illustrated by Fig. 4(d) with $g = 0.22\omega$; (iii) after this intermediate regime, the system performs sinusoidal oscillations again, although its period increases as g increases as can be verified from Figs. 4(e)-(f).

Our goal is to understand the physical description associated to the behavior of the concurrence described above. From our discussion in Sec. III, in view of the characteristics of the anticrossing C' , we expect a dynamics associated with a two-level subspace with the elements being the states $|I\rangle = |\uparrow\downarrow, 00\rangle$ and $|II\rangle = |\downarrow\uparrow, 00\rangle$. Because the effective coupling between $|I\rangle$ and $|II\rangle$ involves second order transitions, we estimate its value applying the perturbation theory, by calculating the matrix element $\Omega = \langle I | H_{\text{eff}} | II \rangle$ defined as

$$\Omega = \langle I | \bar{H}_0 | II \rangle + \sum_{\sigma=\uparrow}^{\downarrow} \sum_{m,l=0}^{\infty} \frac{\mathcal{V}_{I,II}(\sigma, ml)}{\bar{\varepsilon}_{\downarrow\uparrow,00} - \varepsilon_{\sigma\sigma,ml}}, \quad (18)$$

where

$$\mathcal{V}_{I,II}(\sigma, ml) = \langle I | \bar{V} | \sigma\sigma, ml \rangle \langle \sigma\sigma, ml | \bar{V} | II \rangle,$$

We expect that Ω provides the characteristic frequencies found in Fig. 4, which is valid for small values of the coupling g ($g \ll \omega$). The calculation requires the use of a well known property of the displacement operator [73] given by

$$\begin{aligned} \langle ml | \mathbb{D}_{12} | 00 \rangle &= \langle m | D_1(\alpha) | 0 \rangle \langle l | D_2(-\alpha) | 0 \rangle \\ &= e^{-\alpha^2} \frac{\alpha^m}{\sqrt{m!}} \frac{(-\alpha)^l}{\sqrt{l!}}. \end{aligned} \quad (19)$$

After a straightforward calculation, we arrive in the following expression for Ω

$$\Omega = \Omega_0 e^{-2\alpha^2} \sum_{m,l=0}^{\infty} \frac{\alpha^{2m} \alpha^{2l}}{m! l!} \frac{[2\alpha^2 - (m+l)]}{[2\alpha^2 - (m+l)]^2 - (\frac{\delta}{\omega})^2}, \quad (20)$$

where $\Omega_0 = 2|\Delta|^2/\omega$. This effective coupling parameter describes a second order tunneling process, mediated by the electron-vibrational mode interaction.

To check the behavior of Ω , we plot in Fig. 5 the ratio $r = \Omega/\Omega_0$ as function of coupling g , considering the physical conditions associated with anticrossing C' . From our results, we are able to identify three different behaviors: (i) at small values of g , between $g \approx 0$ and $g < 0.18\omega$, $|r|$ increases as g increases; (ii) if $g \approx 0.22\omega$, the factor

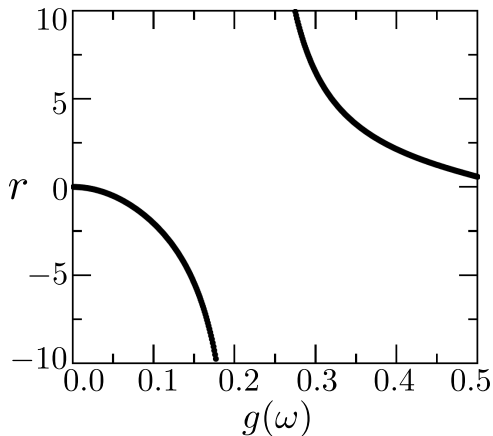


FIG. 5. Ratio $r = \Omega/\Omega_0$ as a function of the electron-vibrational mode coupling, g , as given by Eq. (20), considering the physical parameters of the anticrossing C' : $\Delta = \Delta_1 = \Delta_2 = 5 \times 10^{-3}\omega$ and $\delta = \delta_1 = \delta_2 = 0.1\omega$.

$2\alpha^2$ becomes comparable with δ/ω so the denominator on Eq. (18) goes to infinity if $m = l = 0$. By checking the exact dynamics at this values of g , we realize that the state $\varepsilon_{\uparrow,00}$ becomes resonant with $\varepsilon_{\uparrow\downarrow,00}$ and $\varepsilon_{\downarrow,00}$ so the system evolves to a superposition of this three states and the effective two-level model is no longer valid; (iii) for $0.2\omega < g < 0.5\omega$, the value of $|r|$ decreases as g increases.

At this point, we search for a more detailed characterization of the sinusoidal oscillations. Calculating the evolved state, considering an effective two-level system (2ls) described by $H_{2ls} = \Omega|I\rangle\langle II| + \text{h.c.}$, and the same initial condition used in the numerical analysis, $|\psi_0\rangle = |\uparrow\downarrow, 00\rangle = |I\rangle$, we obtain

$$|\psi(t)\rangle_{2ls} = \cos \Omega t |I\rangle + e^{-i\pi/2} \sin \Omega t |II\rangle, \quad (21)$$

which, in terms of r and θ , is written as

$$|\psi(t)\rangle_{2ls} = \left[\cos(r\theta) |\uparrow\downarrow\rangle + e^{-i\pi/2} \sin(r\theta) |\downarrow\uparrow\rangle \right] \otimes |00\rangle. \quad (22)$$

The analytical expression of the concurrence, considering the effective two-level model, takes the form [76, 78]

$$C_{2ls}(r) = 2|\cos(r\theta) \sin(r\theta)|. \quad (23)$$

In Fig. (4), the behavior of the C_{2ls} is shown using solid gray lines. Notice that Eq.(23) is in good agreement with the full numerical calculations of concurrence. That means that the effective two-level model is able to describe the non-monotonic behavior of the sinusoidal oscillations of the concurrence. In the intermediate range of g 's values, this simplified model does not apply, as $|\Omega| \rightarrow \infty$. Interestingly, though, it catches the fast oscillations observed in Fig. 4(d).

To complete our discussion, we compute the fidelity of the electronic state given by

$$\mathcal{F}(t) = \text{Tr}_{\mathcal{D}}[\rho_{\mathcal{D}}(t)\rho_{\mathcal{D}}^{\text{tar}}], \quad (24)$$

where $\rho_{\mathcal{D}}^{\text{tar}} = |\Psi(\varphi_{\text{tar}})\rangle\langle\Psi(\varphi_{\text{tar}})|$, where $|\Psi(\varphi_{\text{tar}})\rangle$ is defined in Eq.(16a), being φ_{tar} the relative phase of a specific target state. In our simulations, we choose $g = 0.1\omega$ and $g = 0.4\omega$, to explore one example of each range of g with sinusoidal oscillations of Fig. 4.

Our results are shown in Fig. 6, considering two different values for relative phase of the target state: $\varphi_{\text{tar}} = -\pi/2$ (brown dots) and $\varphi_{\text{tar}} = \pi/2$ (black triangles). Notice that the fidelity for both cases of φ_{tar} oscillates out of phase between 0 and 1, and the comparison between them permits to describe accurately the electronic dynamics. Specifically, in Fig. 6(a) considering $g = 0.1\omega$, the initial state $|\uparrow\downarrow\rangle$ evolves to a maximally entangled state of the form $|\Psi(\varphi)\rangle$, which alternates between $|\Psi(\pi/2)\rangle$, at $r\theta = \pi/4$, and $|\Psi(-\pi/2)\rangle$, at $r\theta = 3\pi/4$. Analogously, the results for $g = 0.4\omega$, Fig. 6(b), exhibit the same oscillations, although they are out of phase if compared with Fig. 6(a).

The differences between Fig. 6(a) and Fig. 6(b) are explained by the behavior of ratio r , which goes from negative to positive value depending on the value of g . Considering the evolved state associated with the effective two-level model, Eq.(22), a change on the sign of r implies in a change of the relative phase of the evolved state. Calculating the fidelity of the analytical solution given by Eq.(22), considering the same target state $|\Psi(\varphi_{\text{tar}})\rangle$, it reads as

$$\mathcal{F}_{2ls}(r\theta) = \frac{1}{2} - \cos(r\theta) \sin(r\theta) \sin(\varphi_{\text{tar}}). \quad (25)$$

The evolution of this function is illustrated with the lines in Fig. 6, for each case of g and φ_{tar} , showing good agreement with the numerical results.

V. FEASIBILITY OF THE GENERATION OF ELECTRONIC ENTANGLED STATES

In this section, we review some aspects about physical parameters for the generation of electronic maximally entangled states. The Eq.(23) shows that the concurrence C reaches its first maximum value at $r\theta_{\text{max}} = \pi/4$, which in terms of time scale results in $t_{\text{max}} \approx 1$ ns, for $g = 0.05\omega$ in Fig. 4(a), reducing to $t_{\text{max}} \approx 0.1$ ns, for $g = 0.15\omega$ in Fig. 4(c). To check the robustness of the generation of the entangled states, here we consider the effect of charge dephasing, which is the main mechanism of decoherence in our physical system [3], once our proposal requires low temperatures and small values of excitations on the vibrational modes. We simulate this process solving a master equation [74], where Lindblad operators are introduced to take into account the dephasing of the coherent oscillations in each qubit. The time scale of the dephasing process is given by $T_{\text{deph}} = 1/\gamma_{\text{deph}} = h/\Gamma_{\text{deph}}$, where Γ_{deph} is the dephasing rate, in energy units.

In Fig. 7 we show how concurrence and fidelity evolves in the presence of dephasing, for two different values of Γ_{deph} . The panels (a) and (b) show both quantities con-

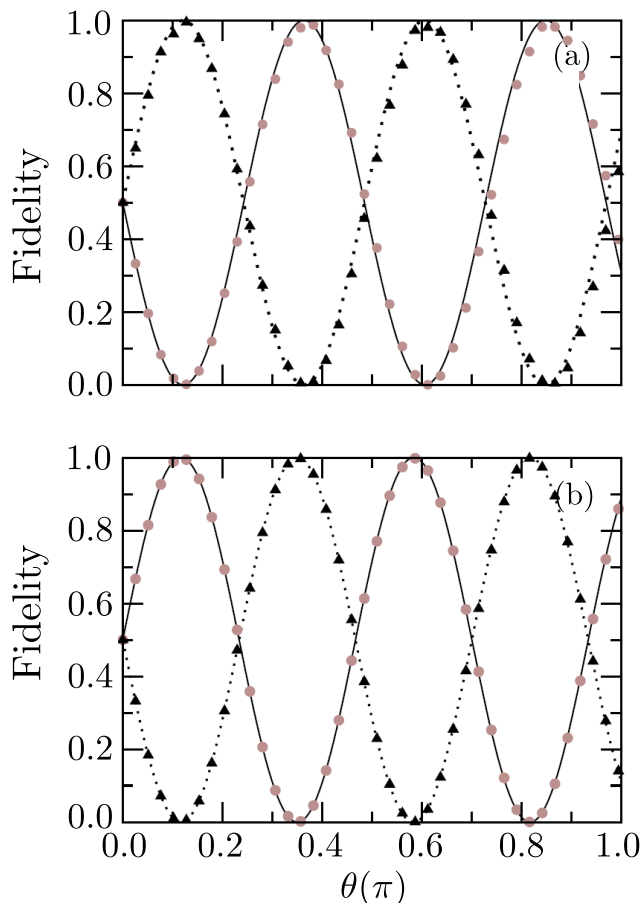


FIG. 6. Evolution of the fidelity, \mathcal{F} , considering the target state $|\Psi(\varphi_{\text{tar}})\rangle$ for two choices of relative phase, $\varphi_{\text{tar}} = -\pi/2$ (brown dots), and $\varphi_{\text{tar}} = \pi/2$ (black triangles). The physical parameters correspond to those considered in Fig. 4 with (a) $g = 0.1\omega$ and (b) $g = 0.4\omega$. Lines show the evolution of $\mathcal{F}_{2\text{ls}}(\theta)$ for the same physical conditions considering $\varphi_{\text{tar}} = -\pi/2$ (solid black line) and $\varphi_{\text{tar}} = \pi/2$ (dotted black line).

sidering $\Gamma_{\text{deph}} = 1 \times 10^{-4}\omega = 2\mu\text{eV}$ (0.5 GHz), while panels (c) and (d) were obtained with $\Gamma_{\text{deph}} = 2 \times 10^{-4}\omega = 4\mu\text{eV}$ (1 GHz). The order of magnitude considered here for Γ_{deph} is in agreement with those reported on feasible experimental scenarios [3, 79, 80].

From the results in Fig. 7, we conclude that our proposal is relatively robust against the process of dephasing, although the entanglement degree and the fidelity present damped oscillation (loss of coherence), the concurrence value for its first maximum is above $C = 0.6$, Figs. 7(a),(c), indicating a high degree of entanglement. Analyzing the evolution of the fidelity in Fig. 7(b),(d), we can conclude that even when a strong dephasing process is considered, the fidelity of the maximally entangled state $|\Psi(\pi/2)\rangle$, given by Eq. (16a), is up to 0.8 in its first peak.

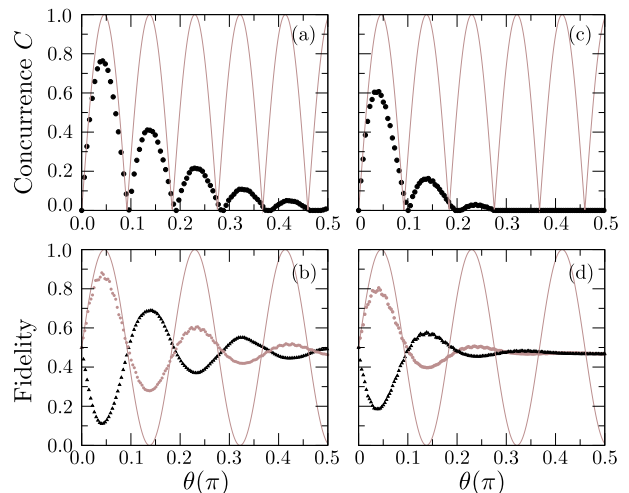


FIG. 7. Evolution of the concurrence and the fidelity, assuming two different values of charge dephasing rate Γ_{deph} , calculated by solving a Lindblad master equation, with $\omega = 20$ meV, $\Delta = 5 \times 10^{-3}\omega = 0.1$ meV and $\delta_1 = \delta_2 = 0.1\omega = 2$ meV, with $g = 0.15\omega = 3$ meV corresponding to the case illustrated in panel (c) in Fig. 4. (a) Concurrence C (black dots) for $\Gamma_{\text{deph}} = 1 \times 10^{-4}\omega = 20 \times 10^{-2}$ meV; (b) fidelity considering the target state $|\Psi(\varphi_{\text{tar}})\rangle$ for two choices of relative phase, $\varphi_{\text{tar}} = -\pi/2$ (brown dots), and $\varphi_{\text{tar}} = \pi/2$ (black triangles), considering the same value Γ_{deph} in panel (a); (c) Concurrence C (black dots) for $\Gamma_{\text{deph}} = 2 \times 10^{-4}\omega = 40 \times 10^{-2}$ meV; (d) Fidelity, also for $\Gamma_{\text{deph}} = 2 \times 10^{-4}\omega$ using the same scheme of colors and symbols of panel (b). In all panels, we illustrate the behavior when the dephasing is neglected (brown solid line).

VI. SUMMARY

We have studied a system of two qubits, encoded in two pairs of quantum dots. Inside each pair, a single electron can tunnel between the quantum dots, thus constituting a two-level system. Electronic degrees of freedom couple to vibrational modes. With the aid of the Lang-Firsov transformation we show that this coupling results in an effective electron-electron interaction, responsible for the creation of highly entangled states. We explore the interplay between electron tunneling, energies detunings and the coupling between electrons and vibrational modes on the formation of entangled states. Our model potentially describes several experimental scenarios, including electrons inside carbon nanotubes quantum dots or the coupling between charged quantum dots and acoustic cavities.

Looking at the spectrum and eigenstates of the present model, we found that, by tuning the electronic levels it is possible to form effective two-level systems that sustain maximally entangled electronic states, such as $|\Psi(\varphi)\rangle$ and $|\Phi(\varphi)\rangle$, as defined in Eq.(16a) and Eq.(16b). For the dynamics, we found that the electronic part of the system can evolve to entangled states for a wide range of

electron-vibrational mode couplings. Interestingly, the frequency of the oscillations on concurrence dynamics behaves in a non-monotonic way as the coupling parameter g increases. Using a perturbation theory that accounts for high order transition processes, we obtain a general expression which provides the characteristic frequencies on the dynamics, although it is valid for small values of the electron-vibrational mode coupling.

VII. ACKNOWLEDGMENTS

We thank the referees for helpful criticism and questions. Their careful and detailed review enriched our paper. This work was supported by CNPq (grant 307464/2015-6), and the Brazilian National Institute of Science and Technology of Quantum Information (INCT-IQ).

Appendix A: The two-qubit Hamiltonian in the rotated Bell-boson basis

The emergence of maximally entangled electronic states on the physical system of interest can be explored by writing down its Hamiltonian in terms of the electronic Bell states. Let us calculate the representation of the original Hamiltonian (1) as a matrix written in the Bell-boson basis $|\psi_{\text{Bell}}, ml\rangle$, where the electronic part is ordered as

$$|\psi_{\text{Bell}}\rangle_{\mathcal{D}} = \{|\Psi_{-}\rangle, |\Phi_{-}\rangle, |\Psi_{+}\rangle, |\Phi_{+}\rangle\}_{\mathcal{D}},$$

. Here

$$\begin{aligned} |\Psi_{\pm}\rangle_{\mathcal{D}} &= \frac{1}{\sqrt{2}} (|\uparrow\downarrow\rangle \pm |\downarrow\uparrow\rangle) \\ |\Phi_{\pm}\rangle_{\mathcal{D}} &= \frac{1}{\sqrt{2}} (|\uparrow\uparrow\rangle \pm |\downarrow\downarrow\rangle), \end{aligned} \quad (\text{A1})$$

are the well known Bell states. We choose to keep together the states with the same number of total excitations $N_{\mathcal{V}\text{T}} = m + l$. This choice remarks the fact that the basis, each value of $N_{\mathcal{V}\text{T}}$ defines a set of subspaces $\mathcal{S}_{\text{B},(ml)}$. Notice that, for $N_{\mathcal{V}\text{T}} = 0$, there is only the subspace $\mathcal{S}_{\text{B},(00)}$ with four states; for $N_{\mathcal{V}\text{T}} = 1$ we have $\mathcal{S}_{\text{B},(10)}$ and $\mathcal{S}_{\text{B},(01)}$ (eight states); $N_{\mathcal{V}\text{T}} = 3$ has twelve states associated with $\mathcal{S}_{\text{B},(11)}$, $\mathcal{S}_{\text{B},(20)}$, and $\mathcal{S}_{\text{B},(02)}$, etc.

Let us write the matrix representation of the Hamiltonian for the first six 4D subspaces $\mathcal{S}_{\text{B},(ml)}$, ordered as $\{\mathcal{S}_{\text{B},(00)}, \mathcal{S}_{\text{B},(01)}, \mathcal{S}_{\text{B},(10)}, \mathcal{S}_{\text{B},(11)}, \mathcal{S}_{\text{B},(02)}, \mathcal{S}_{\text{B},(20)}\}$:

$$H = \left(\begin{array}{ccc|ccc} B_{00} & G_2 & G_1 & 0 & 0 & 0 \\ G_2 & B_{01} & 0 & G_1 & \sqrt{2}G_2 & 0 \\ G_1 & 0 & B_{10} & G_2 & 0 & \sqrt{2}G_1 \\ \hline 0 & G_1 & G_2 & B_{11} & 0 & 0 \\ 0 & \sqrt{2}G_2 & 0 & 0 & B_{02} & 0 \\ 0 & 0 & \sqrt{2}G_1 & 0 & 0 & B_{02} \end{array} \right). \quad (\text{A2})$$

By using the order $|\Psi_{-}, ml\rangle$, $|\Phi_{-}, ml\rangle$, $|\Psi_{+}, ml\rangle$, and $|\Phi_{+}, ml\rangle$, the 4D matrices B_{ml} and G_v are defined as

$$B_{ml} = \begin{pmatrix} E_{ml} & \Delta_{-} & \delta_{-}/2 & 0 \\ \Delta_{-} & E_{ml} & 0 & \delta_{+}/2 \\ \delta_{-}/2 & 0 & E_{ml} & \Delta_{+} \\ 0 & \delta_{+}/2 & \Delta_{+} & E_{ml} \end{pmatrix}, \quad (\text{A3})$$

and

$$G_v = \begin{pmatrix} g_v & 0 & 0 & 0 \\ 0 & g_v/2 & 0 & (-1)^{(v-1)}g_v/2 \\ 0 & 0 & g_v & 0 \\ 0 & (-1)^{(v-1)}g_v/2 & 0 & g_v/2 \end{pmatrix}, \quad (\text{A4})$$

where $E_{ml} = \sum_{i=1,2} \sum_{j=3,4} \sum_{v=1,2} (\varepsilon_i + \varepsilon_j + \omega_v)$ are the energy of the state $|\psi_{\text{Bell}}, ml\rangle$, the tunnel couplings are defined as $\Delta_{\pm} = \Delta_2 \pm \Delta_1$ and $\delta_{\pm} = \delta_1 \pm \delta_2$, with $\delta_{1(2)}$ being the detuning for the qubit 1 (2).

The first matrix resembles the rotated matrix on Bell basis, whose properties discussed in details on Ref. 66, and the matrices G_v depends on g_v and carry on the effect of electron-vibrational mode coupling, where the factor $\sqrt{N_v}$ appears on the specific elements of the matrix (A2) which depends on the values of N_v of the coupled subspaces.

If $\delta_{\pm} = 0$, it seems that the states with electronic part being $|\Psi_{-}\rangle_{\mathcal{D}}$ and $|\Phi_{-}\rangle_{\mathcal{D}}$ are decoupled, at the same time that $|\Psi_{+}\rangle_{\mathcal{D}}$ and $|\Phi_{+}\rangle_{\mathcal{D}}$ are not, in the same way that in Ref. 66. Nevertheless, if elements for the first two lines on matrix (A2), associated with $|\Psi_{-}, 00\rangle$ and $|\Phi_{-}, 00\rangle$ respectively, are written using the notation $|\rangle\langle|$ we obtain:

$$\begin{aligned} H &= |\Psi_{-}, 00\rangle (E_{00} \langle\Psi_{-}, 00| + g_2 \langle\Psi_{-}, 01| + g_1 \langle\Psi_{-}, 10|) \\ &+ |\Phi_{-}, 00\rangle \left(E_{00} \langle\Phi_{-}, 00| + \frac{g_2}{2} \langle\Phi_{-}, 01| - \frac{g_2}{2} \langle\Phi_{+}, 01| + \frac{g_1}{2} \langle\Phi_{-}, 10| + \frac{g_1}{2} \langle\Phi_{+}, 10| \right) + \dots \end{aligned} \quad (\text{A5})$$

We conclude that the term with $|\Psi_{-}\rangle_{\mathcal{D}}$ can be written as $(|\Psi_{-}\rangle\langle\Psi_{-}|)_{\mathcal{D}} \otimes (E_{00}|00\rangle\langle 00| + g_2|00\rangle\langle 01| + g_1|00\rangle\langle 10|)$,

while the others do not permit the same.

Continuing with the calculation, we realize that only

the terms on Hamiltonian associated with $|\Psi_{-}\rangle_{\mathcal{D}}$ are decoupled, at least from the electronic point of view, from the rest of the Bell basis. In this way, there is a Bell state, dressed by vibrational modes, becoming an eigenstate of the Hamiltonian (1) for the specific condition of

$$\begin{aligned} H_{\text{with}|\Psi_{-}\rangle} = & (|\Psi_{-}\rangle\langle\Psi_{-}|)_{\mathcal{D}} \otimes \{ [|\mathbf{00}\rangle_{\mathcal{V}}(E_{00}\langle 00|_{\mathcal{V}} + g\langle 10|_{\mathcal{V}} + g\langle 01|_{\mathcal{V}})] + [|\mathbf{01}\rangle_{\mathcal{V}}(E_{01}\langle 01|_{\mathcal{V}} + g\langle 11|_{\mathcal{V}} + \sqrt{2}g\langle 02|_{\mathcal{V}}) \\ & + |\mathbf{10}\rangle_{\mathcal{V}}(E_{10}\langle 10|_{\mathcal{V}} + g\langle 11|_{\mathcal{V}} + \sqrt{2}g\langle 20|_{\mathcal{V}})] + [|\mathbf{11}\rangle_{\mathcal{V}}(E_{11}\langle 11|_{\mathcal{V}} + \sqrt{2}g\langle 21|_{\mathcal{V}} + \sqrt{2}g\langle 12|_{\mathcal{V}}) \\ & + |\mathbf{02}\rangle_{\mathcal{V}}(E_{02}\langle 02|_{\mathcal{V}} + \dots) + |\mathbf{20}\rangle_{\mathcal{V}}(E_{20}\langle 20|_{\mathcal{V}} + \dots)] + \dots + \text{h.c.} \}. \end{aligned} \quad (\text{A6})$$

Other terms on Hamiltonian cannot be written as a tensorial product of the form $|\psi\rangle\langle\psi|_{\mathcal{D}} \otimes \sum \alpha |m'l'\rangle_{\mathcal{V}}\langle ml|$: terms with $|\Psi_{+}\rangle$ are coupled with $|\Phi_{+}\rangle$ by electron-vibrational mode interaction, while elements $|\Phi_{+}\rangle$ and $|\Phi_{-}\rangle$ are also coupled to each other by tunneling. In the Eq. A6, we use bold type and the square brackets, $[\]$, to emphasize the new Bell-boson basis $\{|\psi_{\text{Bell}}, ml\rangle\}$.

The number of eigenstates per “branch”, i.e. the states belonging to certain value of $N_{\mathcal{VT}}$, and the number of maximally entangled electronic states at $\delta_1 = 0$, are connected with the dimension of original subspaces. Although these subspaces are coupled with each other, each branch can be seen as Bell-boson states, with an energy increasing as $N_{\mathcal{VT}} = m + l$ grows.

Appendix B: Numerical solutions of eigenstates of the Hamiltonian (1) at anticrossings.

In this Appendix, we present our results of the numerical calculation of the eigenstates for the Hamiltonian

equal tunnel couplings, $\Delta_2 = \Delta_1$ and the qubit detunings defined so the condition $\delta_- = 0$. Writing only the terms of the Hamiltonian regarding $|\Psi_{-}\rangle_{\mathcal{D}}$ it is straightforward to see that

(1) at each of the anticrossings discussed in Fig.2. The results are identified by the label used along the discussion in the main text. The physical parameters used in our simulations are consistent with the same figure being $g = 0.1\omega$ and $\Delta_1 = \Delta_2 = 5 \times 10^{-3}\omega$. For each case, the symbol “-” (“+”) denotes the eigenstate with lower (higher) energy from each pair on the anticrossing. For brevity, we suppressed the terms which value is less than 1×10^{-2} .

1. First order anticrossings

- Anticrossing A (for $\delta_2 = 0$):

$$\begin{aligned} |\psi_{A_{-}}\rangle & \approx -0.76 |\downarrow\downarrow, 00\rangle + 0.58 |\uparrow\downarrow, 00\rangle + 0.22 |\uparrow\uparrow, 00\rangle + 0.11 |\downarrow\uparrow, 00\rangle + 0.15 |\downarrow\downarrow, 01\rangle + \dots \\ |\psi_{A_{+}}\rangle & \approx 0.76 |\uparrow\downarrow, 00\rangle + 0.58 |\downarrow\downarrow, 00\rangle - 0.22 |\downarrow\uparrow, 00\rangle + 0.11 |\uparrow\uparrow, 00\rangle - 0.12 |\downarrow\downarrow, 01\rangle + \dots \end{aligned} \quad (\text{B1})$$

- Anticrossing B (for $\delta_2 = 0$):

$$\begin{aligned} |\psi_{B_{-}}\rangle & \approx -0.76 |\uparrow\uparrow, 00\rangle + 0.58 |\downarrow\uparrow, 00\rangle + 0.22 |\downarrow\downarrow, 00\rangle + 0.11 |\uparrow\downarrow, 00\rangle + 0.15 |\uparrow\uparrow, 10\rangle + \dots \\ |\psi_{B_{+}}\rangle & \approx 0.76 |\downarrow\uparrow, 00\rangle + 0.58 |\uparrow\uparrow, 00\rangle - 0.22 |\uparrow\downarrow, 00\rangle + 0.11 |\downarrow\downarrow, 00\rangle - 0.12 |\uparrow\uparrow, 10\rangle + \dots \end{aligned} \quad (\text{B2})$$

- Anticrossing A' (for $\delta_2 = 0.1\omega$):

$$\begin{aligned} |\psi_{A'_{-}}\rangle & \approx 0.70 |\uparrow\downarrow, 00\rangle - 0.70 |\downarrow\downarrow, 00\rangle + 0.14 |\downarrow\downarrow, 01\rangle + \dots \approx [0.70 |\uparrow, 00\rangle - 0.70 |\downarrow, 00\rangle + 0.14 |\downarrow, 01\rangle] \otimes |\downarrow\rangle + \dots \\ |\psi_{A'_{+}}\rangle & \approx 0.70 |\downarrow\downarrow, 00\rangle + 0.70 |\uparrow\downarrow, 00\rangle - 0.14 |\downarrow\downarrow, 01\rangle + \dots \approx [0.70 |\downarrow, 00\rangle + 0.70 |\uparrow, 00\rangle - 0.14 |\downarrow, 01\rangle] \otimes |\downarrow\rangle + \dots \end{aligned} \quad (\text{B3})$$

- Anticrossing B' (for $\delta_2 = 0.1\omega$):

$$\begin{aligned} |\psi_{B'_-}\rangle &\approx 0.70 |\downarrow\uparrow, 00\rangle - 0.70 |\uparrow\uparrow, 00\rangle + 0.14 |\uparrow\uparrow, 10\rangle + \dots \approx [0.70 |\downarrow, 00\rangle - 0.70 |\uparrow, 00\rangle + 0.14 |\uparrow, 10\rangle] \otimes |\uparrow\rangle + \dots \quad (\text{B4}) \\ |\psi_{B'_+}\rangle &\approx 0.70 |\uparrow\uparrow, 00\rangle + 0.70 |\downarrow\uparrow, 00\rangle - 0.14 |\uparrow\uparrow, 10\rangle + \dots \approx [0.70 |\uparrow, 00\rangle + 0.70 |\downarrow, 00\rangle - 0.14 |\uparrow, 10\rangle] \otimes |\uparrow\rangle + \dots \end{aligned}$$

2. Second order anticrossings

- Anticrossing C (for $\delta_2 = 0$):

$$\begin{aligned} |\psi_{C_-}\rangle &\approx 0.70 |\uparrow\downarrow, 00\rangle - 0.70 |\downarrow\uparrow, 00\rangle \approx |\Psi_-\rangle \otimes |00\rangle + \dots \quad (\text{B5}) \\ |\psi_{C_+}\rangle &\approx -0.65 |\uparrow\downarrow, 00\rangle - 0.64 |\downarrow\uparrow, 00\rangle - 0.26 |\uparrow\uparrow, 00\rangle - 0.26 |\downarrow\downarrow, 00\rangle + \dots \end{aligned}$$

- Anticrossing D (for $\delta_2 = 0$):

$$\begin{aligned} |\psi_{D_-}\rangle &\approx -0.64 |\uparrow\uparrow, 00\rangle - 0.64 |\downarrow\downarrow, 00\rangle + 0.27 |\uparrow\downarrow, 00\rangle + 0.27 |\downarrow\uparrow, 00\rangle + 0.13 |\uparrow\uparrow, 10\rangle + 0.13 |\downarrow\downarrow, 01\rangle + \dots \\ |\psi_{D_+}\rangle &\approx -0.69 |\uparrow\uparrow, 00\rangle + 0.69 |\downarrow\downarrow, 00\rangle + 0.14 |\uparrow\uparrow, 10\rangle - 0.14 |\downarrow\downarrow, 01\rangle + \dots \quad (\text{B6}) \end{aligned}$$

- Anticrossing C' (for $\delta_2 = 0.1\omega$):

$$\begin{aligned} |\psi_{C'_-}\rangle &\approx -0.69 |\uparrow\downarrow, 00\rangle - 0.69 |\downarrow\uparrow, 00\rangle + \dots \approx -|\Psi_+\rangle \otimes |00\rangle \quad (\text{B7}) \\ |\psi_{C'_+}\rangle &\approx 0.7 |\uparrow\downarrow, 00\rangle - 0.7 |\downarrow\uparrow, 00\rangle \approx |\Psi_-\rangle \otimes |00\rangle \end{aligned}$$

- Anticrossing D' (for $\delta_2 = 0.1\omega$):

$$\begin{aligned} |\psi_{D'_-}\rangle &\approx 0.69 |\uparrow\uparrow, 00\rangle - 0.69 |\downarrow\downarrow, 00\rangle - 0.14 |\uparrow\uparrow, 10\rangle + 0.14 |\downarrow\downarrow, 01\rangle + \dots \quad (\text{B8}) \\ |\psi_{D'_+}\rangle &\approx -0.69 |\uparrow\uparrow, 00\rangle - 0.69 |\downarrow\downarrow, 00\rangle + 0.14 |\uparrow\uparrow, 10\rangle - 0.14 |\downarrow\downarrow, 01\rangle + \dots \end{aligned}$$

-
- [1] D. Loss and D. P. DiVincenzo, Phys. Rev. A **57**, 120 (1998).
- [2] G. Burkard, D. Loss, and D. P. DiVincenzo, Phys. Rev. B **59**, 2070 (1999).
- [3] X. Zhang, H.-O. Li, G. Cao, M. Xiao, G.-C. Guo, and G.-P. Guo, National Science Review **6**, 32 (2018).
- [4] J. Yoneda, K. Takeda, T. Otsuka, T. Nakajima, M. R. Delbecq, G. Allison, T. Honda, T. Kodera, S. Oda, Y. Hoshi, *et al.*, Nature Nanotechnology **13**, 102 (2018).
- [5] D. M. Zajac, A. J. Sigillito, M. Russ, F. Borjans, J. M. Taylor, G. Burkard, and J. R. Petta, Science **359**, 439 (2018).
- [6] Y. He, S. K. Gorman, D. Keith, L. Kranz, J. G. Keizer, and M. Y. Simmons, Nature **571**, 371 (2019).
- [7] J. R. Petta, A. C. Johnson, J. M. Taylor, E. A. Laird, A. Yacoby, M. D. Lukin, C. M. Marcus, M. P. Hanson, and A. C. Gossard, Science **309**, 2180 (2005).
- [8] J. M. Nichol, L. A. Orona, S. P. Harvey, S. Fallahi, G. C. Gardner, M. J. Manfra, and A. Yacoby, npj Quantum Information **3**, 3 (2017).
- [9] E. A. Laird, J. M. Taylor, D. P. DiVincenzo, C. M. Marcus, M. P. Hanson, and A. C. Gossard, Phys. Rev. B **82**, 075403 (2010).
- [10] T. Hayashi, T. Fujisawa, H. D. Cheong, Y. H. Jeong, and Y. Hirayama, Phys. Rev. Lett. **91**, 226804 (2003).
- [11] X. Mi, S. Kohler, and J. R. Petta, Phys. Rev. B **98**, 161404(R) (2018).
- [12] E. Schöll, L. Hanschke, L. Schweickert, K. D. Zeuner, M. Reindl, S. F. Covre da Silva, T. Lettner, R. Trotta, J. J. Finley, K. Müller, A. Rastelli, V. Zwiller, and K. D. Jöns, Nano Lett. **19**, 2404 (2019).
- [13] H. Borges, L. Sanz, and A. Alcalde, Physics Letters A **380**, 3111 (2016).
- [14] H. S. Borges, L. Sanz, J. M. Villas-Bôas, O. O. Diniz Neto, and A. M. Alcalde, Phys. Rev. B **85**, 115425 (2012).
- [15] M. Russ, D. M. Zajac, A. J. Sigillito, F. Borjans, J. M. Taylor, J. R. Petta, and G. Burkard, Phys. Rev. B **97**, 085421 (2018).
- [16] H. Kiyama, A. Korsch, N. Nagai, Y. Kanai, K. Matsumoto, K. Hirakawa, and A. Oiwa, Scientific Reports **8**, 13188 (2018).
- [17] J. Park, A. N. Pasupathy, J. I. Goldsmith, C. Chang, Y. Yaish, J. R. Petta, M. Rinkoski, J. P. Sethna, H. D.

- Abruña, M. P. L., and D. C. Ralph, *Nature* **417**, 722 (2002).
- [18] G. Shinkai, T. Hayashi, Y. Hirayama, and T. Fujisawa, *Appl. Phys. Lett.* **90**, 103116 (2007).
- [19] G. Shinkai, T. Hayashi, T. Ota, and T. Fujisawa, *Phys. Rev. Lett.* **103**, 056802 (2009).
- [20] D. Xiang, X. Wang, C. Jia, T. Lee, and X. Guo, *Chem. Rev.* **116**, 4318 (2016).
- [21] Y. Xue and M. A. Ratner, *International Journal of Quantum Chemistry* **102**, 911 (2005).
- [22] H. Park, J. Park, A. K. L. Lim, E. H. Anderson, A. P. Alivisatos, and P. L. McEuen, *Nature* **407**, 57 (2000).
- [23] G. A. Steele, A. K. Hüttl, B. Witkamp, M. Poot, H. B. Meerwaldt, L. P. Kouwenhoven, and H. S. J. van der Zant, *Science* **325**, 1103 (2009).
- [24] B. Lassagne, Y. Tarakanov, J. Kinaret, D. Garcia-Sanchez, and A. Bachtold, *Science* **325**, 1107 (2009).
- [25] L. Y. Gorelik, A. Isacsson, M. V. Voinova, B. Kasemo, R. I. Shekhter, and M. Jonson, *Phys. Rev. Lett.* **80**, 4526 (1998).
- [26] A. D. Armour and A. MacKinnon, *Phys. Rev. B* **66**, 035333 (2002).
- [27] A. Donarini, T. Novotný, and A. P. Jauho, *New J. Phys.* **7**, 237 (2005).
- [28] K. V. Kepesidis, M.-A. Lemonde, A. Norambuena, J. R. Maze, and P. Rabl, *Phys. Rev. B* **94**, 214115 (2016).
- [29] S. Walter, B. Trauzettel, and T. L. Schmidt, *Phys. Rev. B* **88**, 195425 (2013).
- [30] J. K. Sowa, J. A. Mol, G. A. D. Briggs, and E. M. Gauger, *Phys. Rev. B* **95**, 085423 (2017).
- [31] R. Leturcq, C. Stampfer, K. Inderbitzin, L. Durrer, C. Hierold, E. Mariani, M. G. Schultz, F. von Oppen, and K. Ensslin, *Nat. Phys.* **5**, 327 (2009).
- [32] M. S. Dresselhaus, G. Dresselhaus, and P. Avouris, *Carbon Nanotubes* (Springer, Berlin Heidelberg, 2001).
- [33] E. A. Laird, F. Pei, W. Tang, G. A. Steele, and L. P. Kouwenhoven, *Nano Lett.* **12**, 193 (2012).
- [34] J. Moser, A. Eichler, J. Güttinger, M. I. Dykman, and A. Bachtold, *Nature Nanotechnology* **9**, 1007 (2014).
- [35] B. J. LeRoy, S. G. Lemay, J. Kong, and C. Dekker, *Nature* **432**, 371 (2004).
- [36] G.-W. Deng, D. Zhu, X.-H. Wang, C.-L. Zou, J.-T. Wang, H.-O. Li, G. Cao, D. Liu, Y. Li, M. Xiao, G.-C. Guo, K.-L. Jiang, X.-C. Dai, and G.-P. Guo, *Nano Lett.* **16**, 5456 (2016).
- [37] J. Chaste, M. Sledzinska, M. Zdrojek, J. Moser, and A. Bachtold, *Applied Physics Letters* **99**, 213502 (2011).
- [38] V. Sazonova, Y. Yaish, H. Üstünel, D. Roundy, T. A. Arias, and P. L. McEuen, *Nature* **431**, 284 (2004).
- [39] K. Jensen, J. Weldon, and A. Zettl, *Nano Lett.* **7**, 3508 (2007).
- [40] H.-Y. Chiu, P. Hung, H. W. C. Postma, and M. Bockrath, *Nano Lett.* **8**, 4342 (2008).
- [41] K. Jensen, K. Kim, and A. Zettl, *Nature Nanotechnology* **3**, 533 (2008).
- [42] A. Benyamini, A. Hamo, S. V. Kusminskiy, F. von Oppen, and S. Ilani, *Nature Physics* **10**, 151 (2014).
- [43] E. A. Laird, F. Kuemmeth, G. A. Steele, K. Grove-Rasmussen, J. Nygard, K. Flensberg, and L. P. Kouwenhoven, *Reviews of Modern Physics* **87**, 703 (2015).
- [44] G. A. Steele, G. Gotz, and L. P. Kouwenhoven, *Nature Nanotechnology* **4**, 363 (2009).
- [45] H. Wang and G. Burkard, *Phys. Rev. B* **92**, 195432 (2015).
- [46] I. I. Rabi, *Phys. Rev.* **49**, 324 (1936).
- [47] I. I. Rabi, *Phys. Rev.* **51**, 652 (1937).
- [48] D. Braak, Q.-H. Chen, M. T. Batchelor, and E. Solano, *Journal of Physics A: Mathematical and Theoretical* **49**, 300301 (2016).
- [49] J. Casanova, G. Romero, I. Lizuain, J. J. García-Ripoll, and E. Solano, *Phys. Rev. Lett.* **105**, 263603 (2010).
- [50] D. Braak, *Phys. Rev. Lett.* **107**, 100401 (2011).
- [51] D. Liwei, H. Shu, D. Braak, and Q.-H. Chen, *Europhysics Letters* **112**, 34003 (2015).
- [52] J. M. Raimond, M. Brune, and S. Haroche, *Rev. Mod. Phys.* **73**, 565 (2001).
- [53] D. J. Wineland, *Rev. Mod. Phys.* **85**, 1103 (2013).
- [54] M. J. Gullans, Y.-Y. Liu, J. Stehlik, J. R. Petta, and J. M. Taylor, *Phys. Rev. Lett.* **114**, 196802 (2015).
- [55] A. Pályi, P. R. Struck, M. Rudner, K. Flensberg, and G. Burkard, *Phys. Rev. Lett.* **108**, 206811 (2012).
- [56] L. Landau and S. Pekar, *J. Exp. Theor. Phys* **18**, 419 (1948).
- [57] D. Emin, *Polarons* (Cambridge University Press, 2012).
- [58] V. N. Stavrou and X. Hu, *Phys. Rev. B* **72**, 075362 (2005).
- [59] S. Vorojtsov, E. R. Mucciolo, and H. U. Baranger, *Phys. Rev. B* **71**, 205322 (2005).
- [60] V. N. Golovach, A. Khaetskii, and D. Loss, *Phys. Rev. Lett.* **93**, 016601 (2004).
- [61] B. Royer, A. L. Grimsmo, N. Didier, and A. Blais, *Quantum* **1**, 11 (2017).
- [62] S. A. Chilingaryan and B. M. Rodríguez-Lara, *Journal of Physics A: Mathematical and Theoretical* **46**, 335301 (2013).
- [63] M. Bina, S. M. Felis, and S. Olivares, *International Journal of Quantum Information* **12**, 1560016 (2014).
- [64] J. Krzywda and K. Roszak, *Scientific reports* **6**, 23753 (2016).
- [65] M. Delbecq, L. Bruhat, J. Viennot, S. Datta, A. Cottet, and T. Kontos, *Nature communications* **4**, 1400 (2013).
- [66] P. Oliveira and L. Sanz, *Ann. Physics* **356**, 244 (2015).
- [67] F. M. Souza and L. Sanz, *Physical Review A* **96**, 052110 (2017).
- [68] K. Goß, M. Leijnse, S. Smerat, M. R. Wegewijs, C. M. Schneider, and C. Meyer, *Phys. Rev. B* **87**, 035424 (2013).
- [69] As pointed out by Sowa *et. al* [30], there can be a phase difference in the coupling parameters g_{v_j} given by where $\phi_{v_j} = \mathbf{k}_{v_j} \cdot \mathbf{d}_{v_j}$, with \mathbf{k}_{v_j} being the wavevector of the j vibrational mode and \mathbf{d}_{v_j} the distance between dots coupled with this specific mode.
- [70] G. D. Mahan, *Many-Particle Physics*, 3rd ed. (Plenum, New York, 2000).
- [71] A. S. Alexandrov and P. E. Kornilovitch, *Phys. Rev. Lett.* **82**, 807 (1999).
- [72] D. M. Kennes, E. Y. Wilner, D. R. Reichman, and A. J. Millis, *Nature Physics* **13**, 479 (2017).
- [73] M. O. Scully and M. S. Zubairy, *Quantum Optics* (Cambridge University Press, 1997).
- [74] T. Fujisawa, G. Shinkai, T. Hayashi, and T. Ota, *Phys. E* **43**, 730734 (2011).
- [75] W. K. Wootters, *Phys. Rev. Lett.* **80**, 2245 (1998).
- [76] S. Hill and W. K. Wootters, *Phys. Rev. Lett.* **78**, 5022 (1997).
- [77] If we consider the values $\varphi, \vartheta = \{0, \pi\}$ we obtain the orthonormal basis for the 4D space given by the Bell

states $|\Psi_{\pm}\rangle$ and $|\Phi_{\pm}\rangle$, defined in Eq.A1.

- [78] C. H. Bennett, D. P. DiVincenzo, J. A. Smolin, and W. K. Wootters, *Phys. Rev. A* **54**, 3824 (1996).
- [79] Z. Shi, C. B. Simmons, D. R. Ward, J. R. Prance, R. T. Mohr, T. S. Koh, J. K. Gamble, X. Wu, D. E. Savage, M. G. Lagally, M. Friesen, S. N. Coppersmith, and M. A. Eriksson, *Phys. Rev. B* **88**, 075416 (2013).
- [80] G. Cao, H.-O. Li, T. Tu, L. Wang, C. Zhou, M. Xiao, G.-C. Guo, H.-W. Jiang, and G.-P. Guo, *Nature communications* **4**, 1401 (2013).